Comparing heat flow models for interpretation of precast quadratic pile heat exchanger thermal response tests

Alberdi-Pagola, Maria; Poulsen, Søren Erbs; Loveridge, Fleur; Madsen, Søren; Jensen, Rasmus Lund

Comparing heat flow models for interpretation of precast quadratic pile heat exchanger thermal response tests

Maria Alberdi-Pagola*, Department of Civil Engineering, Aalborg University.
Søren Erbs Poulsen, VIA Building, Energy & Environment, VIA University College.
Fleur Loveridge, School of Civil Engineering, University of Leeds.
Søren Madsen, Department of Civil Engineering, Aalborg University.
Rasmus Lund Jensen, Department of Civil Engineering, Aalborg University.

*Corresponding author:
M. Alberdi-Pagola
E-mail address: mapa@civil.aau.dk
Address: Department of Civil Engineering, Thomas Manns Vej 23, 9220 Aalborg Ø, DK.

Abstract

This paper investigates the applicability of currently available analytical, empirical and numerical heat flow models for interpreting thermal response tests (TRT) of quadratic cross section precast pile heat exchangers. A 3D finite element model (FEM) is utilised for interpreting five TRTs by inverse modelling. The calibrated estimates of soil and concrete thermal conductivity are consistent with independent laboratory measurements. Due to the computational cost of inverting the 3D model, simpler models are utilised in additional calibrations. Interpretations based on semi-empirical pile G-functions yield soil thermal conductivity estimates statistically similar to those obtained from the 3D FEM inverse modelling, given minimum testing times of 60 hours. Reliable estimates of pile thermal resistance can only be obtained from type curves computed with 3D FEM models. This study highlights the potential of applying TRTs for sizing quadratic, precast pile heat exchanger foundations.

Key words

Thermal response test, pile heat exchanger, heat flow model, inverse modelling, thermal conductivity, pile thermal resistance.

1. Introduction

Ground source heat pump (GSHP) systems are sustainable and cost effective space conditioning systems based on shallow geothermal energy [1]. Utilisation of geothermal energy supports the reduction of the greenhouse gas emissions proposed by the Paris Agreement within the United Nations Framework Convention on Climate Change [2].

Sizing guidelines for closed loop horizontal and vertical ground heat exchangers have been developed over the last decades (Figure 1, a and b) [3][4]. Several factors must be taken into consideration when dimensioning GSHP installations including the dynamics of the cooling and heating demands of the building, the thermal properties of the soil and the backfilling material, the geometry and spacing of the ground heat exchangers, the thermal influence of the ground surface and the presence of groundwater flow, if any (Figure 1).
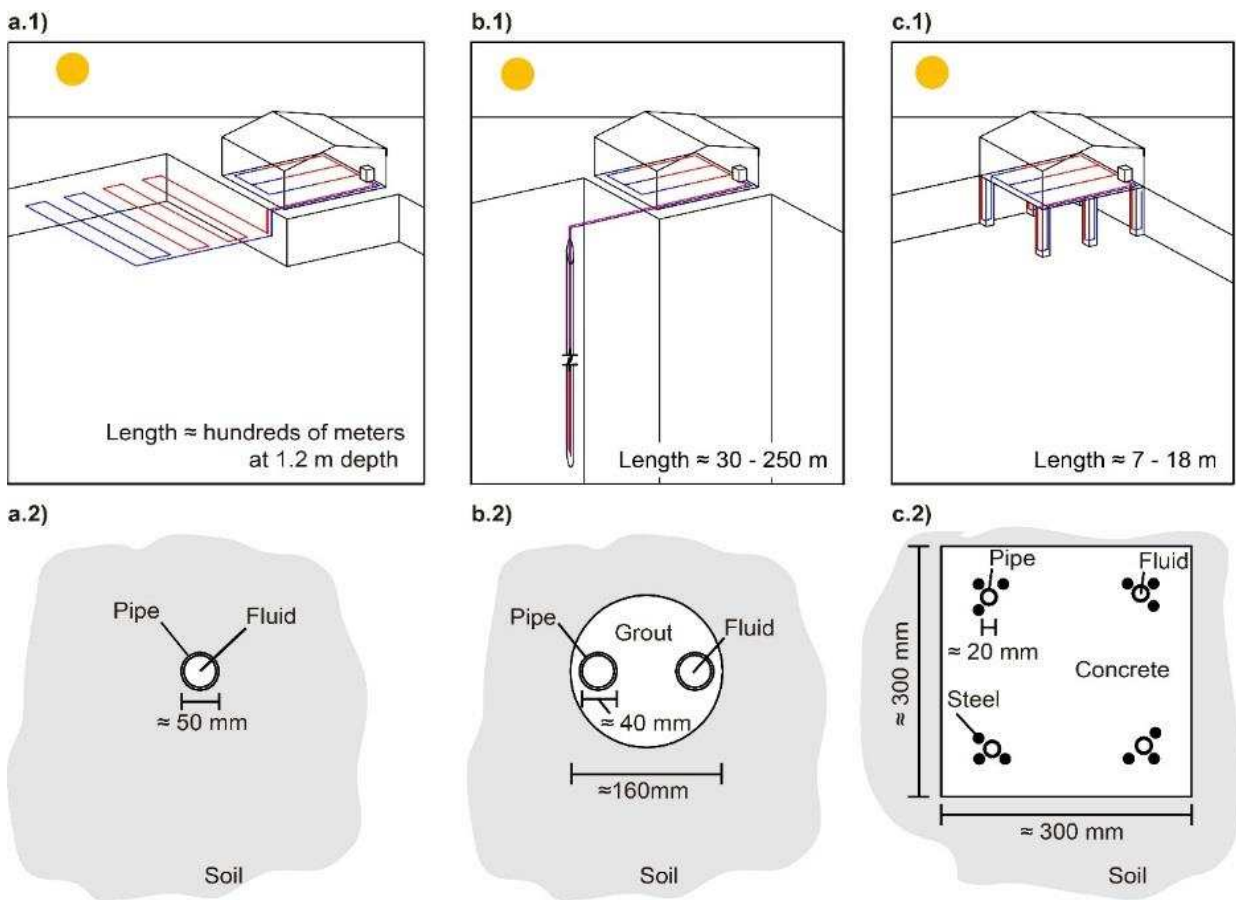
Figure 1: Closed loop ground source heat pump GSHP systems: a.1) GSHP system based on horizontal heat exchangers; a.2) horizontal heat exchanger cross section; b.1) GSHP system based on vertical borehole heat exchangers; b.2) borehole heat exchanger cross section; c.1) GSHP systems based on pile heat exchangers and c.2) precast pile heat exchanger cross section.

Foundation pile heat exchangers were developed during the 1980's as an alternative to traditional borehole heat exchangers [5] (Figure 1, c). Pile heat exchangers, typically referred to as energy piles, consist of traditional foundation piles with embedded heat exchanger pipes. Energy piles differ from conventional borehole heat exchangers by their length and cross section, being both shorter and wider, and materials. Energy pile aspect ratios (length/diameter) are typically less than 50, while for traditional borehole heat exchangers aspect ratios range 200-1500.

Pile heat exchangers vary in length from 7 to 50 m with a cross section of 0.3 to 1.5 m. The methods of construction include: cast-in-place concrete piles, 0.3-1.5 m in diameter [6][7][8][9]; precast concrete piles with side lengths spanning 0.27-0.6 m [10][11][12][13]; hollow concrete precast piles [14] and driven steel piles [15][16].

1.1. Thermal Response Testing

Dimensioning of vertical ground heat exchangers such as boreholes and energy piles requires the determination of the soil thermal conductivity, λ_s [W/m/K], and heat exchanger thermal resistance, R_b [K·m/W]. The thermal conductivity λ_s is a measure of the ease with which soil conducts heat, while the heat exchanger thermal resistance R_b is the integrated thermal resistance between the GSHP carrier fluid and the ground; it serves as an efficiency measure for the heat exchanger. For borehole heat exchangers these parameters are usually determined in situ using thermal response testing (TRT) of one or more ground heat exchangers [17][18][19]. During the TRT, the heat carrier fluid (water) is circulated in the ground heat exchanger while being continuously heated at a specified rate. Heat dissipates to the ground heat exchanger and subsequently to the ground. The test records fluid inlet- and outlet temperatures, the fluid flow rate and energy consumption and logs them in 10-minute intervals for at least 48 hours (Figure 2).
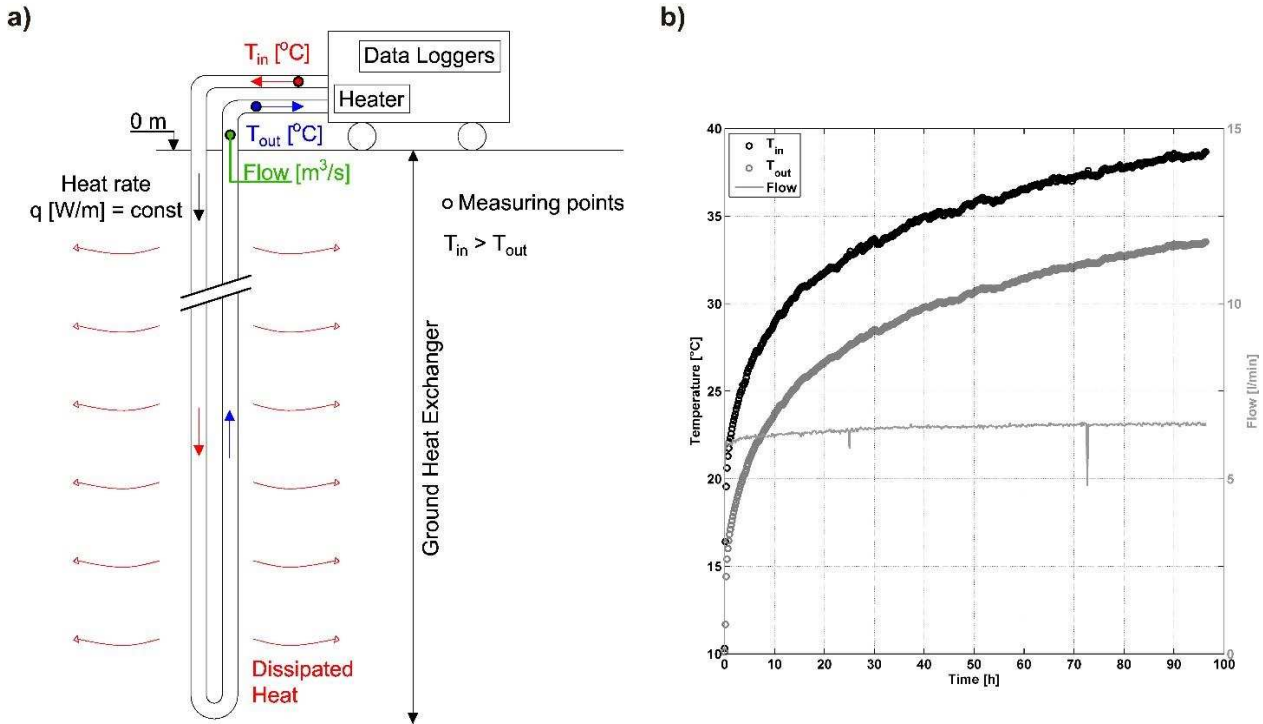
Figure 2: Thermal response test TRT process: a) TRT setup and principle of the in-situ test, after [18]; b) Typical TRT measurements.

The TRT data is evaluated by regression methods applied to analytical, semi-empirical or numerical models designed to link the heat applied to the ground heat exchanger and the resulting temperature change. Due to its simplicity, the most widely used method of interpretation is based on the infinite line source (ILS) model [20]. However, there is a wide range of heat flow models that describe heat transport in the heat exchanger and the soil, including the infinite cylinder source model [21] and the finite line source model [22][23]. These models assume thermal steady-state conditions in the borehole heat exchanger. More complex models, such as the composite medium line source [24] and

the infinite and finite solid cylinder source models [25] account for the heat capacity of the heat exchanger. For further details see [26], [19] and [27].

The uncertainty on line-source based TRT estimates of soil thermal conductivity is in the order of ± 10% [18]. Ref. [28] demonstrated that propagation of measurement errors for TRTs is expected to be approximately 5% for the soil thermal conductivity λ_s and 10-15% for the borehole resistance R_b. Ref. [29] showed that the line-source analysis provides reliable results under ideal simulated situations however the added effects of model simplification errors are up to 10%.

1.2. Pile Thermal Response Testing

Occasionally, the TRT method has been adopted for analysing the thermal behaviour of energy piles [30]. Table 1 provides a summary of previous research in which the TRT has been deployed for estimating the soil thermal conductivity λ_s and the pile thermal resistance (called R_p herein). Ref. [31], [32], [30] and [33] suggest that the TRT is applicable to piles with a diameter less than 0.3 m. Testing times increase for larger piles due to the greater thermal mass of the heat exchanger.

Table 1: Summary of pile heat exchanger TRT studies. The concrete cover is defined as the distance from the pipe edge to the pile wall.

Pile type, pipe configuration*	Dimensions [m]: length, diameter or size, concrete cover	TRT duration	Interpretation methodology**	Soil thermal conductivity λ_s [W/m/K]	Pile thermal resistance R_p [K·m/W]	Deviation from reference values λ_s***	Ref.
Precast square, 1U	12.0, 0.27 x 0.27, 0.10	30 h	ILS	2.56	0.170	22% higher than BHE TRT	[16]
Cast-in-place, W	45.0, 0.60, 0.13	48 h	ILS	2.96	-	-	[34]
		48 h	CCM	2.42	-		
Cast-in-place, 2U	18.3, 0.305, 0.09	96 h	G-function ts	2.90	0.061	From -3% lower to 20% higher than lab	[7], data from [8]
Cast-in-place, 1U	18.3, 0.305, 0.09	67 h	G-function ts	3.45	0.104		
Cast-in-place, 2U	18.3, 0.457, 0.16	100 h	G-function ts	3.20	0.104		
Cast-in-place, 1U	18.3, 0.457, 0.16	110 h	G-function ts	3.55	0.135		
Cast-in-place, 1U	26.8, 0.30, 0.08	72 h	G-function	2.40	0.125	-	[33]
		72 h	ILS	2.60	0.125		
Cast-in-place, 1U	16.1, 0.60, 0.05	72 h	ILS	4.19	-	Considered inaccurate.	[35]
		72 h	2D FEM λ_s parameter change	1.20 - 2.00	-	Within range of lab (1.50 - 2.40)	
Precast square, 2U	17.0, 0.35 x 0.35, -	120 h	ILS	2.70	0.160	15 % higher than lab	[36]
Cast-in-place, 2U	20.0, 0.62, 0.11	110 h	CaRM inverse analysis	1.50	0.120	-	[37]
		110 h	ILS	2.80	-	-	

*1U: Single-U; 2U: Double-U; 3U: Three-U; W: W-shape (continuous pipe).
**ILS: Infinite Line Source; CCM: Composite Cylindrical Model; FEM: Finite Element Model, CaRM: Capacity Resistance Model; ts: time superposition.
***BHE: borehole heat exchanger.

The ILS model has been used in previous studies to evaluate TRT data from energy piles [16], [14], [34], [33], [35], [36], [37]. Depending on the geometry of the pile, line source model simplifications potentially bias estimates of soil thermal conductivity and pile thermal resistance by neglecting three-dimensional effects and the thermal dynamics of the pile. The ILS based interpretation overestimates soil thermal conductivity as measured temperatures tend to fall below the line source modelled temperatures due to vertical heat transport. In previous research ILS estimates of soil thermal

conductivity exceed corresponding values obtained with the composite cylinder model [34], capacitance models [37] and numerical models [35] by 22%, 80% and 230%, respectively.

Ref. [35] analyse TRT data with 2D FEM temperature models of horizontal cross sections of a cylindrical energy pile seated in geological layers with contrasting thermal properties. The authors find soil thermal conductivities in agreement with the laboratory derived values (Table 1). However, [35] ignores vertical heat transport and heat loss at the foot of the pile in their modelling. Refs. [16], [7] and [36], listed in Table 1, report higher values of soil thermal conductivity than the lab- or in-situ derived values, up to 22% [16], 20% [7] and 15% [36]. Determining the pile thermal resistance requires further analysis.

1.3. Scope of this study

In this study, five TRTs of quadratic cross section energy piles carried out in Denmark are interpreted with analytical, semi-empirical and numerical models by means of non-linear regression. Initially, soil thermal conductivity is estimated by inverse 3D FEM modelling of the TRT data and then compared to corresponding, independent laboratory measurements. A fully 3D based TRT interpretation is not feasible for routine practical applications, due to the immense computational burden of solving the inverse problem, which could last days. Consequently, the study also explores the applicability of simpler analytical and semi-empirical models for interpretation of the TRT data. The tested models include the infinite and finite line and cylinder (hollow and solid) source models and the empirically-based G-functions (see e.g. [38]).

2. Experimental data

The precast quadratic cross section energy piles studied in this paper have so far been used in Denmark [39], Germany [40] and Austria [41]. Figure 3 shows the studied energy pile with W-shaped and single-U pipe heat exchangers, respectively. The length of these precast piles is usually limited to 18 m due to transportation logistics.
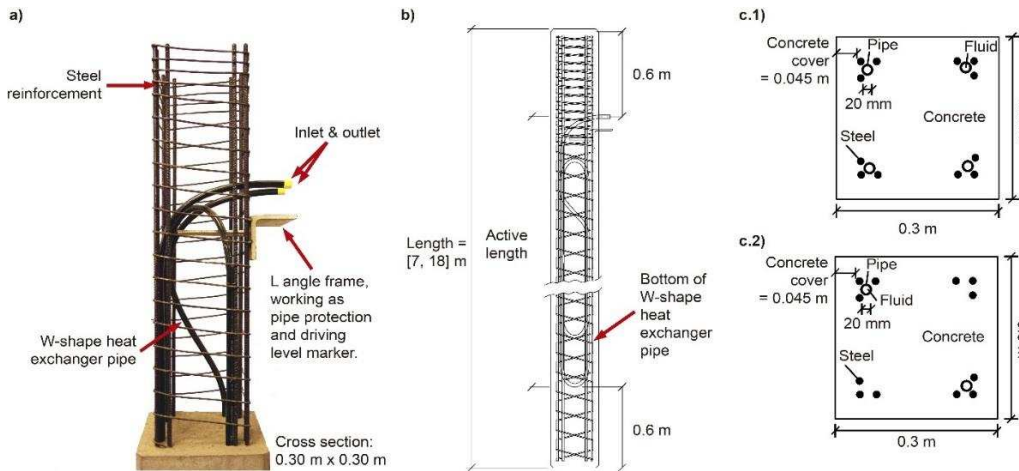
Figure 3: a) Demonstration model of the precast energy pile with W-shaped heat exchanger pipes fitted to the reinforcement bars; b) vertical profile; c.1) horizontal cross section of the W-shape energy pile and; c.2) horizontal cross section of the single-U energy pile.

The data analysed have been collected from two different locations in Denmark: the Langmarksvej test site in Horsens (55° 51′ 43″ N, 9° 51′ 7″ E) where three energy piles have been tested and the Rosborg test site in Vejle (55° 42′ 30″ N, 9° 32′ 0″ E), with two tested energy piles. The experimental data

consist of TRT temperatures and laboratory measurements of the thermal properties of soil and concrete samples. The test sites and the field work are further described in [42].

2.1. Thermal Response Test data

Five TRTs were performed on energy piles differing in length and the configuration of the geothermal piping (W-shaped and single-U, refer to Table 2). The dimensionless TRT temperatures Φ (Equation 1) are plotted in Figure 4 with corresponding Fourier numbers Fo (Equation 2).

$$\Phi = \frac{2\pi\lambda_s\Delta T}{q} \tag{1}$$

$$Fo = \frac{\alpha_s t}{r_b^2} \tag{2}$$

where q [W/m] is the heat injection rate normalized by the active length of the heat exchanger, ΔT [K] is the temperature change between the undisturbed soil temperature T_0 [°C] and the measured average fluid temperature T_f [°C], α_s is the thermal diffusivity [m²/s], i.e., the ratio between the thermal conductivity λ_s and the volumetric heat capacity ρc_p [J/m³/K], t [s] is the time and r_b [m] is the pile radius. The corresponding laboratory estimates of soil thermal conductivity λ_s are used in Equation 1. In Equation 2, the pile radius r_b is the radius that provides an equivalent circumference to the square perimeter. This radius closely maintains the position of the pipes and the concrete cover within the pile cross section, as compared to the quadratic cross section shown in Figure 3, c.1. The five TRT data sets are available in [dataset] [43].
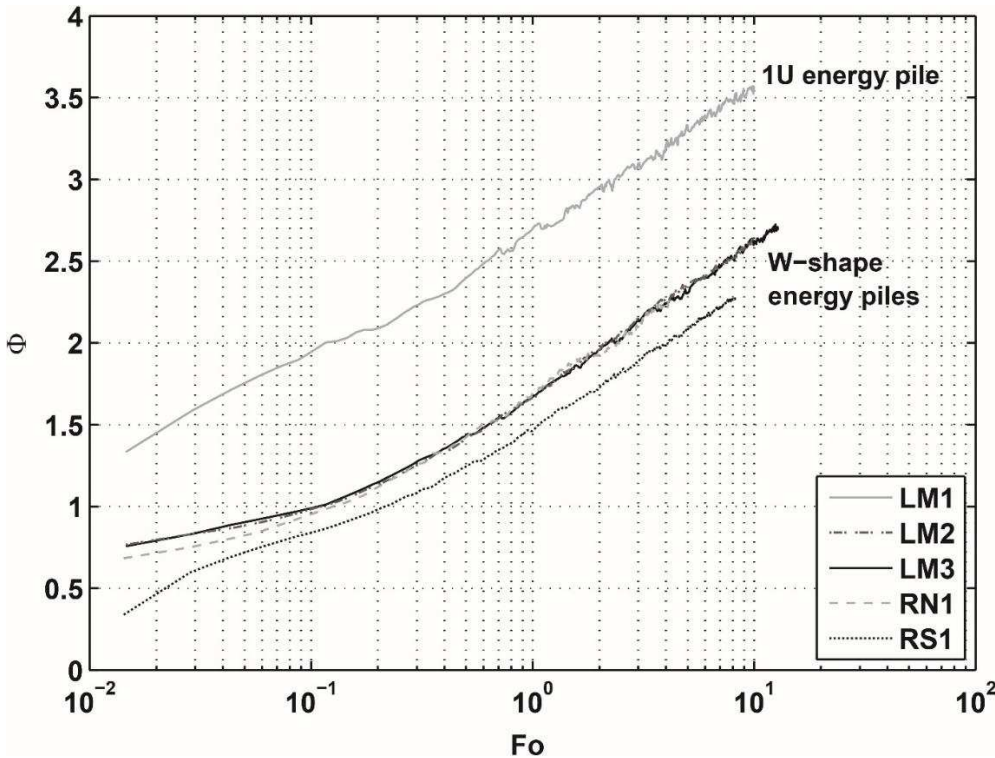

Figure 4: Dimensionless, average fluid TRT temperatures. The pile IDs and correspond details are provided in Table 2.

Test parameters are summarised in Table 2.

Table 2: Test parameters for the five TRTs. The quadratic cross section piles have a side length of 30 cm. The measurement interval was 10 min. The outer and inner diameters of the PEX pipes are 2 cm and 1.6 cm, respectively and water serves as the heat carrier fluid. The piping between the TRT instrument and the tested piles (1.2 m approx.) is carefully insulated to reduce ambient temperature effects.

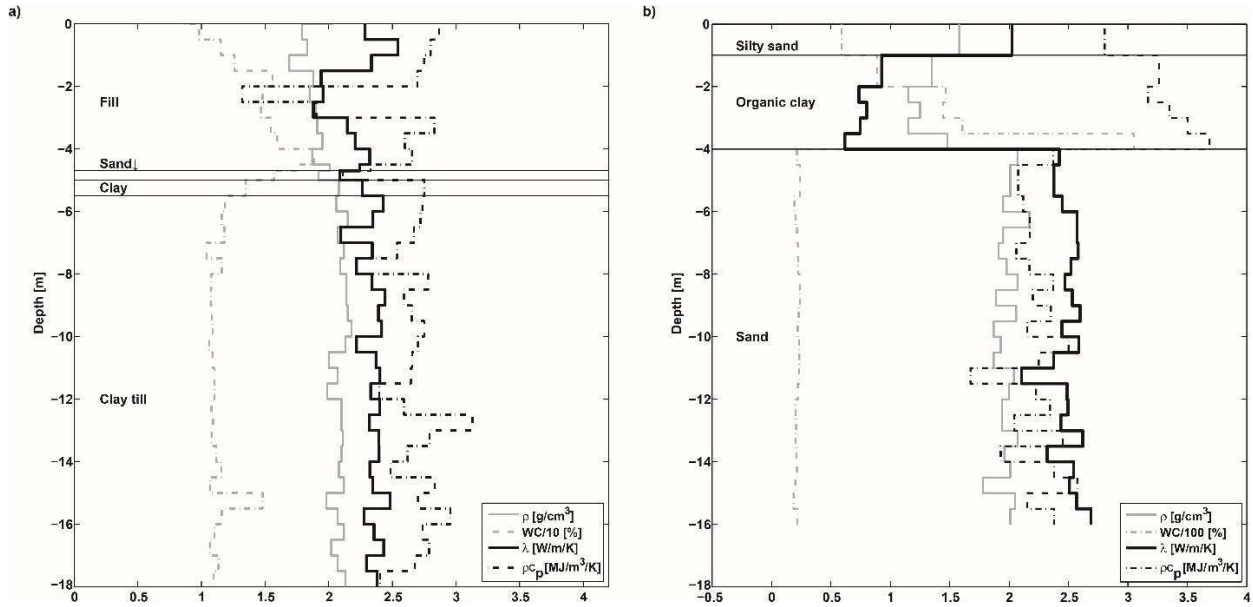| Test site	Langmarksvej (LM)	Langmarksvej (LM)	Langmarksvej (LM)	Rosborg South (RS)	Rosborg North (RN)
Pile heat exchanger ID	LM1	LM2	LM3	RS1	RN1
Heat exchanger pipe configuration	1U	W	W	W	W
Active length [m]	10.8	10.8	16.8	15.0	14.8
Aspect ratio (AR = active length/diameter)	28	28	44	39	39
Undisturbed soil temperature T_0 [°C]	12.1	11.4	10.4	10.2	9.9
Volumetric flow rate [m³/h]	0.50	0.56	0.51	0.39	0.54
Average heat injection rate q [W/m]	101.4	159.4	167.6	152.5	157.8
Heat injection rate, standard deviation as % of average	4.3	4.7	3.7	4.3	3.1
TRT duration [h]	120	114	147	96	49

2.2. Laboratory measurements

The thermal properties of the soil and the concrete have been measured with a Hot Disk apparatus which measures the sample thermal conductivity and diffusivity with an accuracy of ± 5% and ± 10%, respectively [44]. Five repeated measurements were performed on each sample at a room temperature (20 to 23 °C).

Soil samples were collected every 50 cm from borings at both test sites. The samples were immediately placed in sealed bags and tested within 48 hours. The cohesive samples were kept intact while for the non-cohesive samples, the natural water content was preserved, as best possible.

The borehole at Langmarksvej is located approximately 90 cm from the energy pile LM3 and 5-6 m from piles LM1 and LM2. At Rosborg the drilling is placed 50 m and 100 m from RN1 and RS1, respectively. The test site at Langmarksvej show 4-5 m of man-made fill topping glacial clay till. Glacial sand and gravel situated at 5-6 m below terrain are topped by postglacial organic clay at the Rosborg test site. Table 3 provides the layer-thickness-weighted arithmetic mean of the measured characteristics, with full results for the soil borings shown in Figure 5.

Table 3: Summary of the laboratory measurements. The thermal conductivity and volumetric heat capacity are estimated by the layer-weighted arithmetic mean of the measurements over the active length of the heat exchanger.

Material	Bulk density [kg/m³]	Thermal conductivity λ [W/m/K]	Volumetric heat capacity ρc_P [MJ/m³/K]
Soil, Langmarksvej (18 m deep drilling)	2030	2.30 ± 0.13	2.61 ± 0.27
Soil, Rosborg North (16 m deep drilling)	1850	2.14 ± 0.11	2.47 ± 0.29
Concrete, oven dry (0% water content in mass)	2320	2.30 ± 0.28	1.69 ± 0.29
Concrete, saturated (4% water content in mass)	2410	2.75 ± 0.15	2.37 ± 0.28

Figure 5: Density, water content, thermal conductivity and volumetric heat capacity profiles at the a) Langmarksvej and b) Rosborg test sites. Depth is relative to the ground surface. Notice that the plotted water content is scaled differently for the two test sites.

The concrete samples were measured in both dry and saturated conditions to infer the range of feasible thermal conductivities and diffusivities. The laboratory measurements are summarised in Table 3.

3. Methods

The 3D FEM model is described first and the selected analytical, empirical and numerical models are presented afterwards. Lastly, the parameter estimation procedure, applied to all the models, is described.

3.1. Finite element model

The software COMSOL Multiphysics has been used to calculate the subsurface temperature response in and near the energy pile [45]. COMSOL solves the governing Equation 3 for transient thermal conduction in solids by means of the finite element method:

$$\rho c_p \frac{\partial T}{\partial t} = \nabla(\lambda \nabla T) + Q \tag{3}$$

where ρc_p [J/m³/K] is the volumetric heat capacity, T [K] the temperature, t [s] the time, λ [W/m/K] is the bulk thermal conductivity tensor and Q [W/m³] is the heat generation rate. The presence of groundwater flow is ignored in the simulations and the ground is assumed to be thermally isotropic and homogeneous. The thermal interaction of the pile heat exchanger with the surrounding soil is modelled by conduction (heat transfer within concrete and soil) and advection in the heat exchanger pipes. The 3D model contains three domains (Figure 6): the soil, the concrete pile and the heat exchanger pipe, embedded in the concrete, which contains the fluid. The upper 60 cm of the pile do not contain heat exchanger pipes and are not included in the model (see Figure 3).
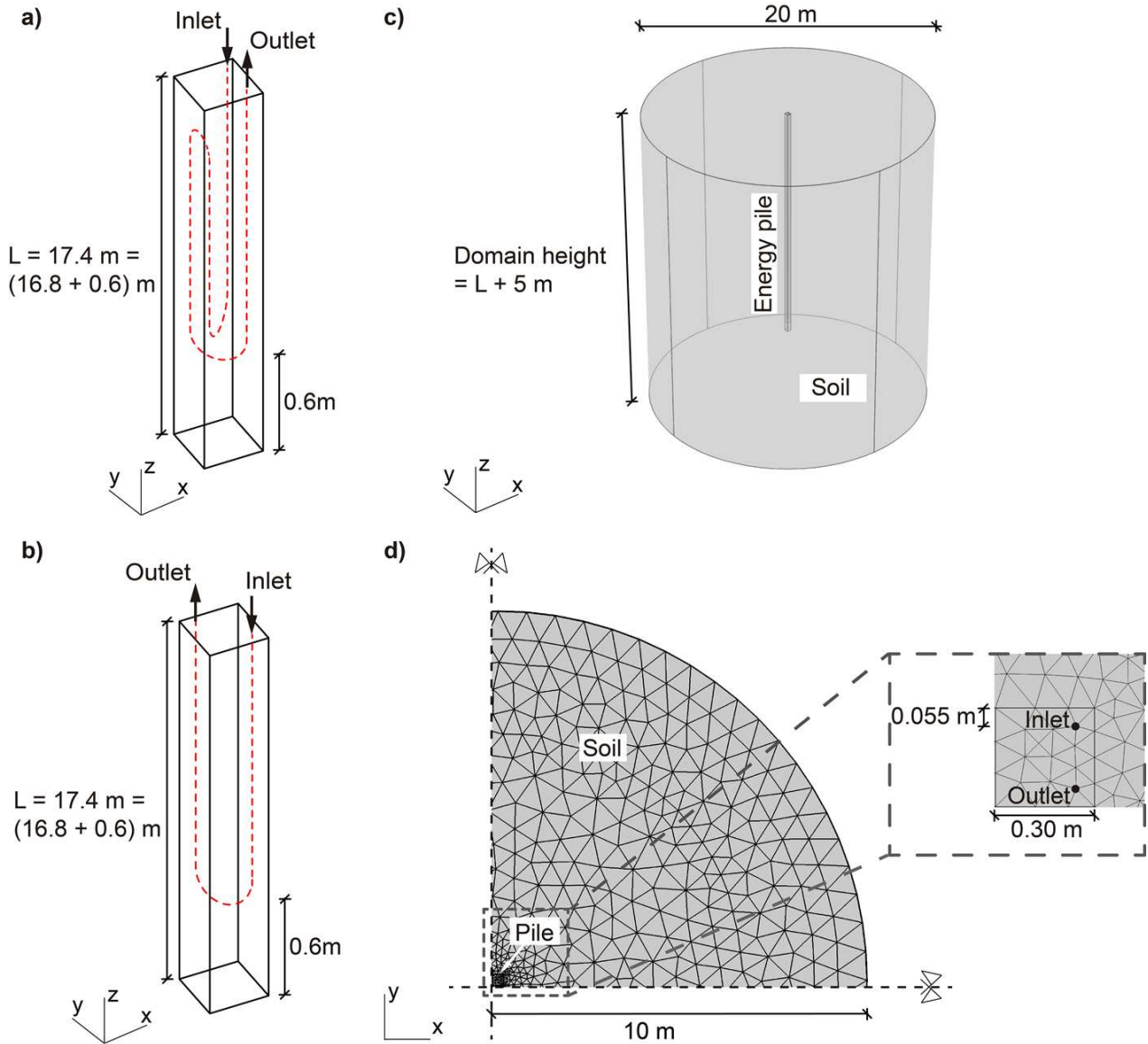
Figure 6: Description of the 3D finite element model simulated in COMSOL: a) Schematic of the W-shape pile heat exchanger; b) Schematic of the Single-U pile heat exchanger; c) Simulated meshed domains; d) Top view of a quarter of domain.

The 3D model utilises two modules in COMSOL: transient heat transfer in solids (applied to all the domains) and non-isothermal pipe flow (applied to the pipe). The non-isothermal pipe flow model approximates advective, 1D transport of heat by the circulating heat carrier fluid in hollow tubes along lines represented in 2D or 3D [46]. The 1D simplification is justified due to the high slenderness ratio of the heat pipe. It is assumed that the velocity profile is fully developed, it does not change within a section, and a negligible temperature change within the pipe in the radial direction occurs. This avoids the more challenging mesh compatibility of the full pipe cross section and the 3D solid materials since edge elements are used to solve for the tangential cross-section averaged velocity. Turbulent pipe flow is specified in accordance with the actual TRT conditions. The diameter of the PEX pipe is 20 mm with a wall thickness of 2 mm and the thermal conductivity of the pipe material is 0.42 W/m/K. Flow in the pipe simulated with Churchill's friction model [47] which accounts for the internal advective thermal resistance. Both the W-shaped and the single-U pipe configurations are modelled (Figure 6a and 6b).

The thermal effects of the steel reinforcement bars are negligible as shown by [48] and [49], and as such they are not included in the modelling.

Model tests were made to ensure that modelled temperatures are independent of chosen level of temporal and spatial discretisation and to ensure that the simulated temperature changes at the boundaries are negligible. The model extends 20 m horizontally and from the surface to 5 m below the energy pile (Figure 6). The mesh is refined in the immediate vicinity of the pile. A fine mesh with tetrahedral, prismatic, triangular, quadrilateral, linear and vertex elements has been created. The minimum element size is 3.4 cm and the maximum element size is 78.4 cm.

The initial temperature in the model domain is set equal to the undisturbed ground temperature measured prior to the TRT. Specified temperature conditions equal to the measured initial temperature are imposed at the soil domain boundaries. The measured inlet temperature during the TRTs is specified for the inlet node of the pipe (Figure 6d).

3.1.1. Model verification

The 3D FEM modelled temperatures are compared to short- and long-time pile-wall temperature responses calculated with existing analytical models including finite and infinite line and solid cylinder sources (see Section 3.2 for model details) in Figure 7.
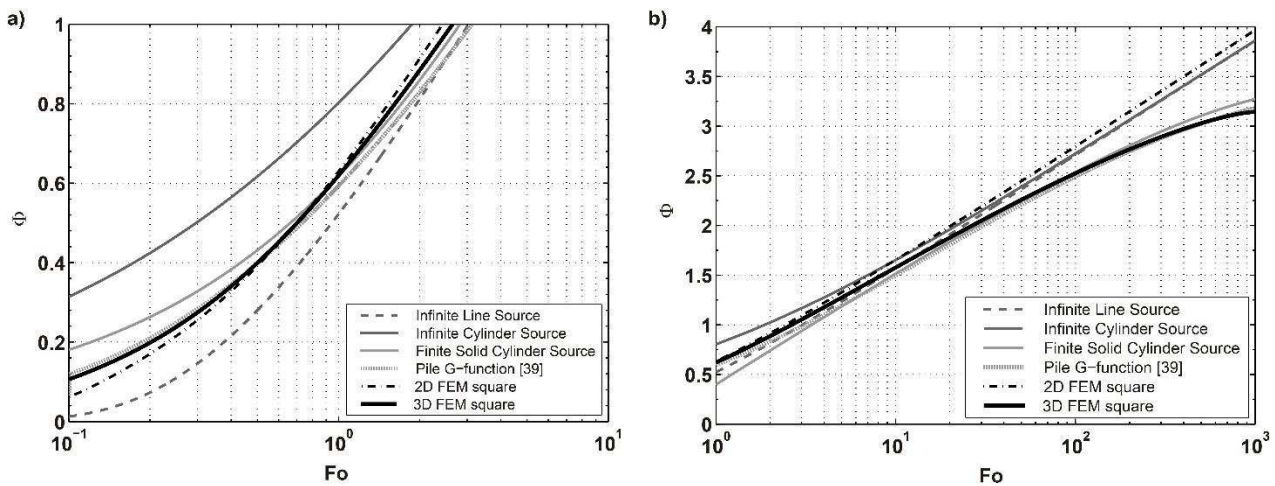
Figure 7: Pile wall temperature responses for the 3D finite element model and selected corresponding analytical models assuming an aspect ratio of 44. a) Short-term and b) long-term responses.

The curves are computed assuming a constant heat injection rate considering identical soil and concrete thermal conductivities. The temperature change θ is defined as the difference between the initial soil temperature T_0 and the computed average pile wall temperature T_b.

The largest difference in calculated, normalised temperatures between the 3D finite element model and the finite source is 0.17 for Fo = 900. This corresponds to a temperature difference of 0.90 °C at approximately 415 days. This discrepancy is considered acceptable since analytical solutions do not capture the influence of the square cross section and 3D effects such as the thermal short circuiting between pipes, causing overestimated long-term temperatures. As shall be seen in Section 4.1, the 3D FEM model also allows excellent representation of the field results, providing full confidence in its suitability for the inverse analysis.

3.1.2. Pile thermal resistance

The thermal conductivity of the concrete largely impacts the pile thermal resistance R_p [K·m/W], which also depends on the position, size and number of pipes, the circulating fluid and flow regime and the dimensions of the pile. Pile thermal resistance is defined as:

$$R_p = \frac{T_f - T_b}{q} \qquad (4)$$

where T_f [°C] is the average fluid temperature and T_b [°C] is the pile heat exchanger average wall temperature computed from the 3D finite element model and q [W/m] is the heat injection rate normalized by the active length of the heat exchanger. To uncouple the influence of the convective heat transfer within the pipes, the term pile concrete thermal resistance R_c [K·m/W] is defined. It is determined from subtracting the convective and conductive resistances of the pipe R_{pipe} from the pile thermal resistance [38], [50]:

$$R_c = R_p - R_{pipe} \qquad (5)$$

$$R_{pipe} = \frac{1}{2n\pi r_i h_i} + \frac{\ln(r_o/r_i)}{2n\pi\lambda_{pipe}} \qquad (6)$$

where n is the number of pipes in the pile heat exchanger cross section, r_i [m] is the inner radius of the pipe, r_o [m] is the outer radius of the pipe, h_i [W/m^2/K] is the heat transfer coefficient and λ_{pipe} [W/m/K] is the thermal conductivity of the PEX pipe. R_c can also be determined as:

$$R_c = \frac{T_p - T_b}{q} \qquad (7)$$

where T_p [°C] is the average temperature on the outer wall of the pipe.

3.2. Selected analytical, empirical and numerical heat flow models

The investigated models comprise analytical models, where the heat transfer in the ground heat exchanger is assumed to be in steady-state and semi-empirical and numerical models, where transient heat transfer in the ground heat exchanger is considered. The models are listed in Table 4 and are further described in Table A.1 in Appendix A. The finite line source model is not considered as it does not differ significantly from the ILS solution for the considered testing times [51] and aspect ratios between 25 and 50.

Table 4: Summary of models selected to evaluate the pile heat exchanger TRT data.

	Model description and reference	Analysed time range
Analytical approaches	Infinite line source ILS by [52].	Fo > 5, steady state in the pile.
	Infinite cylinder source ICS by [21]. The simplification by [53] is used in this study.	Fo > 5, steady state in the pile.
	Infinite solid cylinder source ISCS by [25].	Fo > 4, steady state in the pile.
	Finite solid cylinder source FSCS by [25].	Fo > 4, steady state in the pile.
Semi-empirical approach	G-function for pile heat exchangers (G-flov) by [38]. The finite length of the pile is considered. Variable heating rates can be considered by time superposition (G-flovts).	Fo > 0.1, transient in the pile.

Numerical approaches	Equivalent pipe model EQpipe by [54]. The model presented in [55] is used in this study. The model neglects the finite length of the pile.	Fo > 0, transient in the pile.
	2D horizontal cross section FEM 2D FEM developed for this study. It neglects the finite length of the pile.	Fo > 0, transient in the pile.

G-functions are dimensionless, time dependent temperature response functions for computing the temperature T_b on the energy pile wall (shown here in their general form):

$$T_b = \frac{q}{4\pi\lambda_s} G(r = r_b, Fo) \tag{8}$$

where G is the G-function. All the analytical expressions in Table 4 and Appendix A can be expressed in this form. Additionally, in this study the semi-empirical pile G-functions [38] were also used. These were estimated by 3D modelling of cylindrical energy piles. In all cases the average fluid temperature in the heat exchanger pipes is calculated as:

$$T_f = T_0 + qR_p + T_b \tag{9}$$

For the analytical models qR_p is constant since the pile is assumed steady. For the pile G-functions qR_p is also a function of Fo, as set out in Appendix A. When time variations of the heat rate need to be considered, the temperature change is computed as:

$$\Delta T_n = \sum_{i=1}^{i=n} \frac{q_i}{2\pi\lambda_s} \left(G\left(Fo_n - Fo_{(i-1)}\right) - G\left(Fo_n - Fo_{(i)}\right) \right) \tag{10}$$

where n is the point in normalised time in which the superposition is evaluated.

3.3. Parameter estimation

The parameter estimation is performed with PEST Model-Independent Parameter Estimation software [56]. PEST employs the Gauss-Marquardt-Levenberg algorithm for minimizing the weighted, squared difference between computed and observed fluid temperatures. PEST calculates linear confidence intervals for estimated parameter following the non-linear regression procedure.

For the 3D FEM inverse modelling, the measured outlet temperatures serve as calibration data assigned with equal observation weights. The average of the late-time in- and outlet temperatures ($t_c > 5r_b^2/\alpha$) serve as calibration data for the analytical models. In the interpretation of the TRT of RN1, the aforementioned time criterion was lowered by a factor of 1.5 due to the short duration of the test. All measured temperatures are considered in the calibration of the semi-empirical and numerical models. The initial parameter values in the parameter estimation are set equal to the corresponding laboratory measurements (Table 3). The thermal conductivities are allowed to vary from 1.0 to 3.5 W/m/K while the volumetric heat capacities in the 3D FEM model are constrained to ±10% of the corresponding laboratory measurements. For the analytical approaches, the pile thermal resistance R_p is restricted to 0.01-0.3 K·m/W. For the semi-empirical approach the pile concrete thermal resistance R_c is allowed to vary between 0.01 and 0.30 K·m/W.

12

4. Results and discussion

Firstly, the 3D FEM calibrated parameter estimates are compared to corresponding laboratory measurements. Secondly, the estimated parameters from calibration of the heat flow models listed in Section 3.2 are compared to corresponding estimates obtained from the inverse 3D FEM modelling and discrepancies are discussed. Next, the pile thermal resistance in the context of square cross section energy piles is further explored. Finally, recommendations on applying TRT in the dimensioning of quadratic cross section precast pile heat exchanger foundations are provided.

4.1. 3D FEM parameter estimation and concrete thermal resistance

The 3D FEM modelling closely matches the observed outlet fluid temperatures as shown in Figure 8 for the case of pile LM3.
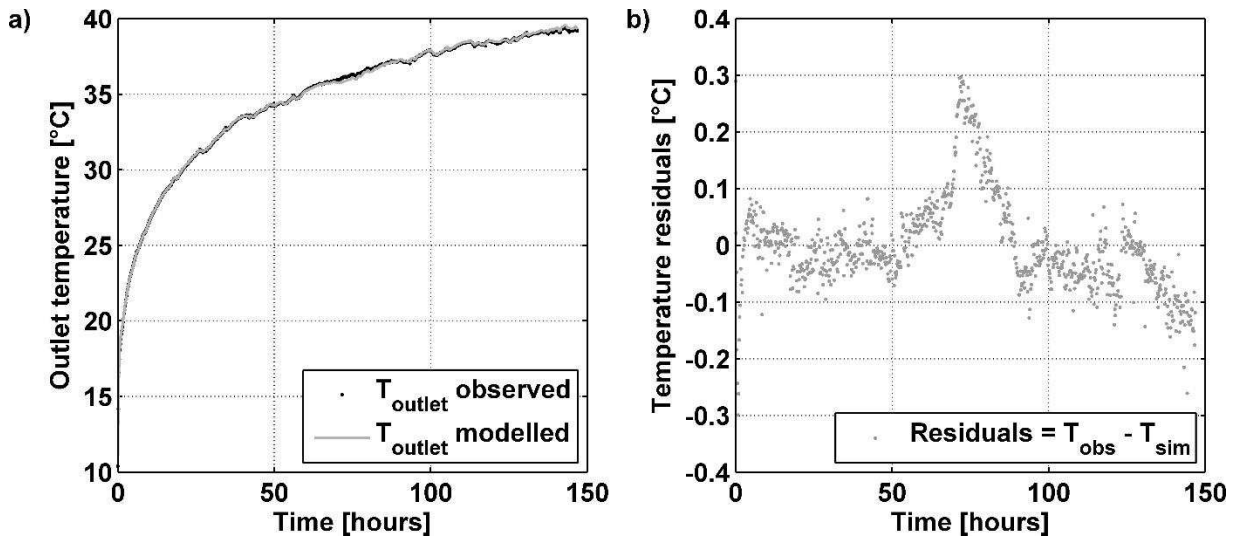

Figure 8: Model calibration of LM3. a) Observed and modelled outlet temperatures; b) residuals, defined as the difference between the observed and the simulated temperatures.

The resulting thermal conductivity values from the inverse calculations are given for all piles in Table 5.

Table 5: Calibration estimates and linear 95% confidence levels for the soil and concrete thermal conductivities determined from 3D FEM.

Energy pile ID	Thermal conductivity soil λ_s [W/m/K]	Thermal conductivity concrete λ_c [W/m/K]	Root Mean Squared Error RMSE
LM1	2.50 ± 0.16	2.33 ± 0.19	0.036
LM2	2.21 ± 0.05	2.85 ± 0.14	0.029
LM3	2.22 ± 0.07	2.46 ± 0.15	0.083
RN1	2.20 ± 0.22	2.35 ± 0.19	0.065
RS1	2.21 ± 0.06	3.05 ± 0.13	0.047

Figure 9 compares the inverse 3D FEM modelling estimates with the laboratory measurements. Overlapping confidence bounds, demonstrate good agreement between computed estimates and the laboratory conductivity measurements. The estimates of soil thermal conductivity are consistent with

geological profiles that show similar geology nearby the tested piles [57]. The estimated concrete thermal conductivity for RS1 slightly exceeds the laboratory measurements. While the concrete production process is strictly controlled, it is not unlikely that some compositional variation exists between different batches of concrete.
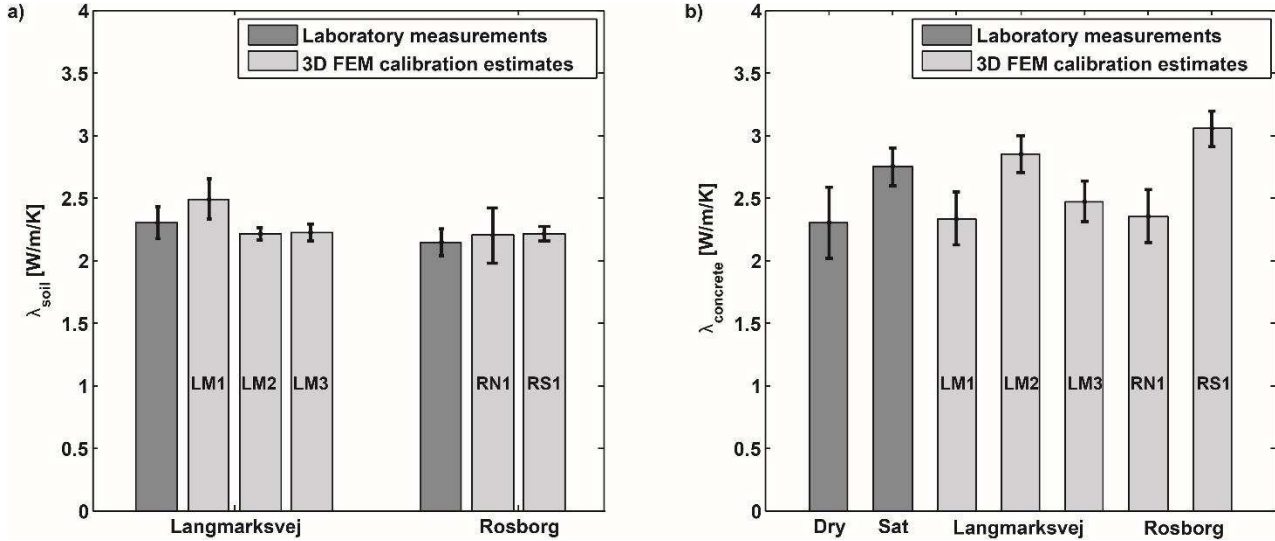
Figure 9: Laboratory measurements of thermal conductivity compared to 3D model calibration estimates. a) Soil thermal conductivity with weighted, averaged laboratory measurements; b) concrete thermal conductivity, "Sat" indicates saturated conditions. The error bars correspond to the 95% linear confidence intervals.

Previous research indicate that TRT based soil conductivity estimates exceed corresponding laboratory measurements [58], [59], [60]. The inconsistency is attributed to drilling and sampling methods, variations in the natural moisture content, thermal anisotropy and variations in confining pressure. Advanced interpretation methods, such as inverse 3D finite element modelling, yield better agreement between laboratory and calibrated conductivity estimates (Table 1). Therefore, if sufficient caution is taken in the sampling and measuring processes and adequate interpretation methods are used, the influence of the aforementioned factors are minimised. It is concluded that the inverse 3D FEM modelling provides accurate estimates of the thermal conductivity of the soil and the concrete.

The 3D FEM computed average pile wall temperature forms the basis for estimating the pile concrete thermal resistance following equation 7 (Table 6).

Table 6: 3D FEM model based estimates of concrete thermal resistance R_c.

Pile ID	LM1	LM2	LM3	RN	RS
R_c [K·m/W]	0.095	0.045	0.045	0.049	0.039

The W-shaped and single-U pile heat exchangers yield an average concrete thermal resistance R_c of 0.044 and 0.095 K·m/W, respectively.

4.2. Comparison with simpler heat flow models

The inversion of the 3D FEM model is associated with excessive computational time (days), rendering it impractical for routine interpretation. It is therefore investigated to what extent simplifications of the forward model influence parameter estimates. The models described in Section 3.2 form the basis

for reinterpretations of the five TRTs to compare calibration estimates to those of the inverse 3D FEM modelling.

Figure 10 shows parameter estimates from calibration of simpler, numerical, analytical and semi-empirical heat flow models, normalised by the 3D FEM results (Table 5).
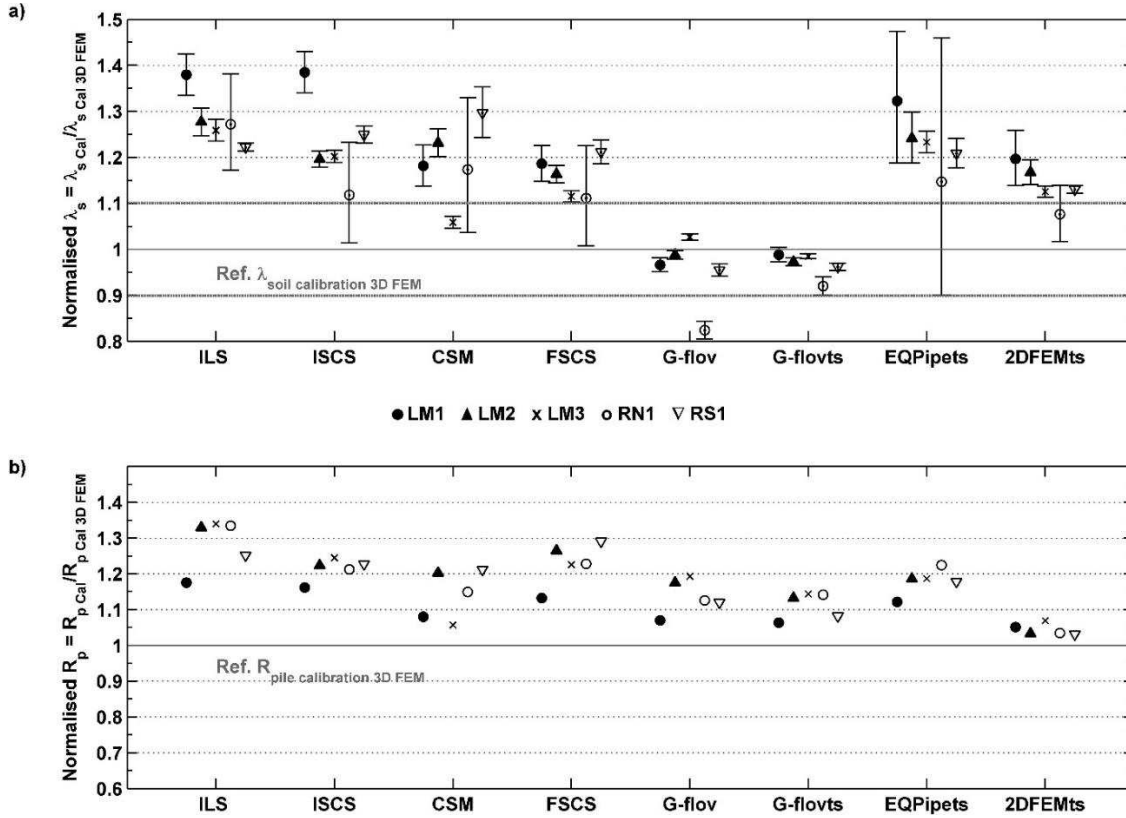
Figure 10: Parameter estimates from calibration of the heat flow models normalised by the 3D FEM based estimates. G-flovts accounts for variable heating rates. a) The uncertainty bounds depicted (grey) in a) correspond to the largest uncertainty obtained in the calibration of the 3D FEM models (test RN1). b) Uncertainties are not shown for the pile thermal resistance R_p as they are insignificant (order of 10^{-2} K·m/W).

Models that do not account for the initial transient behaviour (both finite and infinite approaches) tend to overestimate the thermal conductivity of the soil λ_s by up to 38% for the single-U pile LM1 and up to 25% for W-shape pile heat exchangers, relative to the reference values (Figure 10a). This discrepancy is greater for the single-U pile due to its larger pile resistance. The time superposition G-function (G-flovts) model was also calibrated to take into account heating fluctuations during the TRTs. Both G-flov and G-flovts estimates consistently fall within the uncertainty of the 3D FEM estimates although slightly underestimating the reference value. The maximum difference of 8% for the model G-flovts is obtained for the RN1 test (pile RN1), which relative to the four other test, has the shortest duration and the largest parameter estimate uncertainties.

As temperature responses of the infinite source models eventually become linear in logarithmic time, the lower, actual temperatures due to downward heat loss, are compensated for by increasing the soil thermal conductivity in the parameter estimation (refer to Figure 7). The difference in 2D and 3D FEM modelled temperatures for Fo=10 exceed 5% for the LM3 pile with an aspect ratio of 44 and the deviation is expected to increase for lower aspect ratios. This is in accordance with the findings in [38].

For the G-functions by [38] temperatures fall slightly below those of the 3D FEM model causing a slight underestimation of the soil thermal conductivity.

Figure 10b shows the estimated pile thermal resistance R_p. Generally, the models consistently overestimate the concrete thermal resistance, up to 35% for the ILS model. The 2D FEM model provides the closest match however it systematically overestimates the reference value by 5 to 9%. This model considers the square cross section of the pile but it does not take into account the convective resistance associated with pipe fluid flow (first term on right-hand side of Equation 6). The higher measured temperatures during the initial hours (refer to 2D FEM curve in Figure 7), result in a lower estimated thermal conductivity of concrete λ_c, compared to the 3D FEM estimate. This yields a higher pile thermal resistance R_p.

For the analysed models, the thermal conductivity of the soil λ_s and the pile thermal resistance R_p are positively correlated implying that the parameters can be increased simultaneously without seriously compromising the model fit to measured temperatures. Consequently, the systematic overestimation of the soil thermal conductivity illustrated in Figure 10a is compensated for by increasing the thermal resistance of the pile in the model calibration.

4.3.   Concrete thermal resistance

The pile concrete thermal resistance R_c measures the efficiency of the ground heat exchanger in steady state conditions (Equation 5). The time required for establishing steady-state conditions in the pile was computed with the 3D FEM model (Figure 11).
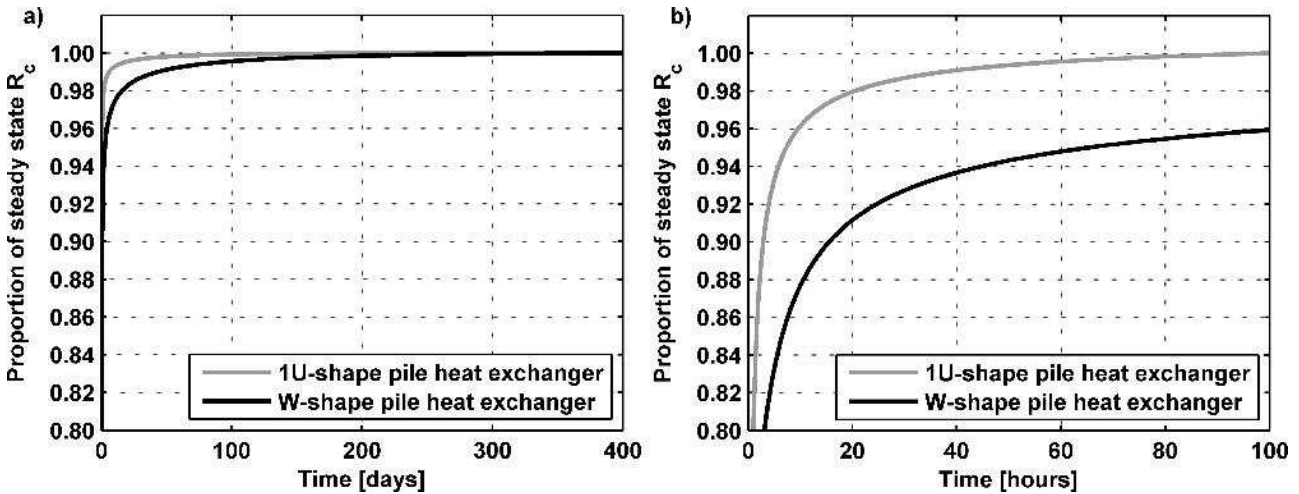

Figure 11: Evolution of pile concrete thermal resistance Rc over time, computed with the 3D finite element model as synthetic TRT data: a) Long-term behaviour and b) Short-term zoom.

Steady-state conditions exist in the single-U pile after 100 hours of testing while 96% of the steady-state concrete thermal resistance is reached for the W-shaped heat exchanger pile. As such, the TRT of RN1 (49 hours) most likely was too short yielding the greatest deviation and uncertainty on estimated parameters (Figure 10).

The investigations presented in the previous sections have not provided reliable models for estimating the pile concrete thermal resistance R_c. Therefore, the pile concrete thermal resistance must be estimated with the 3D FEM model. Imposing a constant heat injection rate in steady state conditions, upper and lower bounds of the concrete thermal resistance R_c for different λ_c/λ_s ratios are computed, for single U- and W-configuration energy piles. The upper bound corresponds to a λ_c/λ_s ratio of 2, while

the lower bound corresponds to a λ_c/λ_s ratio of 0.5. 7 m and 18 m are considered as upper and lower bounds on the pile length, respectively. The calculated concrete thermal resistances R_c are shown in Figure 12.
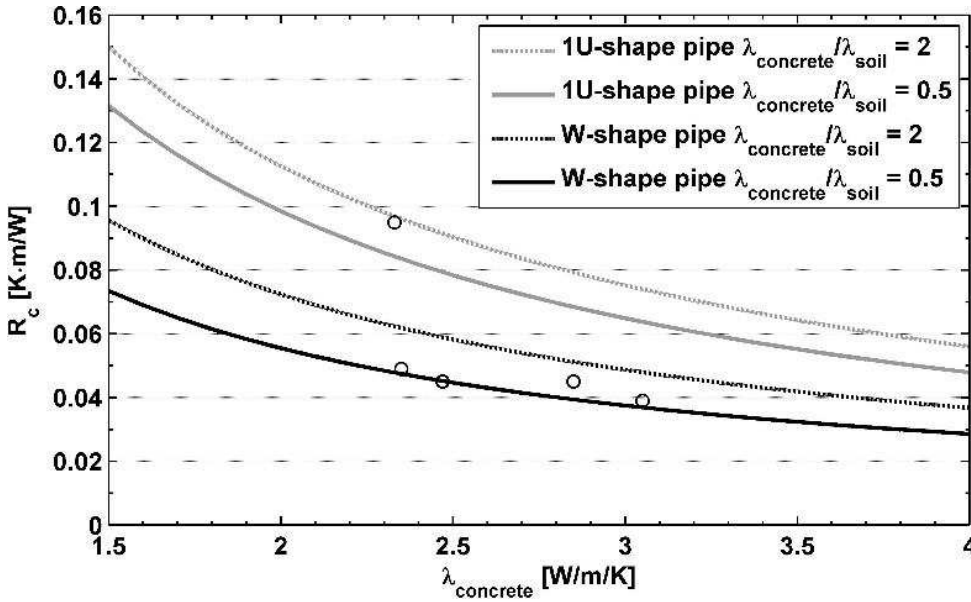

Figure 12: Upper and lower bounds for the concrete thermal resistance R_c for square precast pile heat exchangers with single-U- and W-shape pipes obtained from 3D FEM modelling for a range of concrete thermal conductivities. Calibrated 3D FEM model based estimates of R_c are indicated with circles.

The computed curves for 7 m and 18 m piles differ only slightly and, therefore, the most conservative estimates are shown for the single U and W-shape pipes in Figure 12. The thermal resistance is higher for single-U energy piles and decreases as the thermal conductivity of the concrete increases. The TRT estimates obtained from the 3D FEM calibration (Table 6), indicated with circles in Figure 12, fall within the computed resistance bounds, as expected. Concrete thermal resistance varies moderately for the expected range of concrete thermal conductivity (approx. 2.3 to 3.1 W/m/K). Within this range, the thermal conductivity of the soil barely affects the concrete thermal resistance (less than 13%).

4.4. Testing times

The G-functions proposed by [38] provide consistent soil thermal conductivity λ_s values for the five TRTs analysed. It is of interest to examine plots of the stepwise estimates of soil thermal conductivity for the five TRTs. Sequential plots give indications as to whether calibrated conductivities converge to a particular value as further data are included in the interpretation. Figure 13 shows the calibrated soil thermal conductivity at different testing times: the initial time is 10 hours with a time increment of 30 minutes in the stepwise interpretation of the five TRTs.
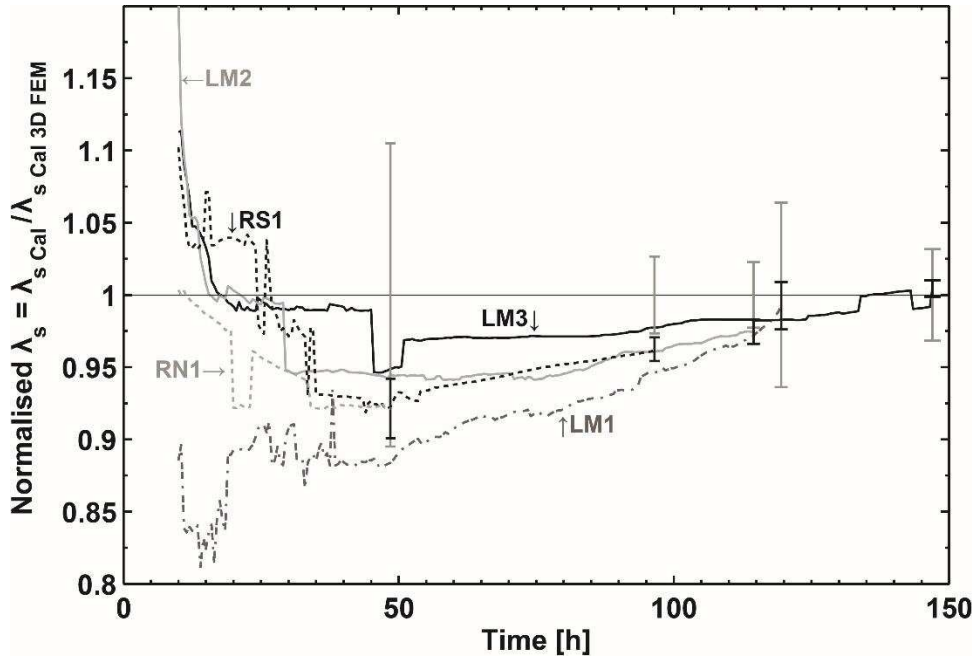
Figure 13: Stepwise interpretation of the five TRTs with the G-functions proposed by [39] and with corresponding soil thermal conductivity estimates. The time increment is 30 minutes. Error bars are indicated for the duration of the test: black) uncertainty bands for the G-flovts calibrated estimates; grey) uncertainty bands for the 3D FEM calibrated estimates.

The duration of the analysed TRTs in this study range from 49 to 150 hours (i. e., Fourier's number 4.5 to 10). As shown in Figure 13, the G-functions by [39] yield estimates of soil thermal conductivity λ_s that fall well within the 3D FEM uncertainty bounds. Beyond 100 hours, the G-function calibrated conductivities converge to the corresponding 3D FEM estimate, suggesting that testing times should be longer than 120 hours. However, G-function and 3D FEM modelled temperatures tend to diverge at later times (see Figure 7) which potentially leads to overestimation of the soil thermal conductivity λ_s. Hence, dimensionless testing times for the studied precast pile heat exchangers should not exceed Fo = 10 (150 hours) nor be less than Fo = 5 (60 hours, approximately). The 49-hour TRT of pile RN1 is likely to be too short (Fo < 4.5).

5. Conclusions

We apply 3D finite element models to interpret five thermal response tests of square cross section foundation pile heat exchangers (energy piles) with contrasting lengths and pipe configurations. The FEM model accepts measured fluid inlet temperatures as input and computes outlet temperatures. The interpretation procedure is based on inverse modelling of observed outlet temperatures to estimate the bulk thermal conductivity of the soil and the concrete. The 3D finite element model accurately reproduces the observed outlet temperatures of the TRTs and estimates are in close agreement with corresponding laboratory measurements. The pile concrete thermal resistances are computed from the simulated pipe and pile wall temperatures, respectively.

Due to immense computational burden of calibrating the 3D model, the TRTs are reinterpreted with simpler analytical, empirical and numerical models. Parameter estimates from the reinterpretation of soil thermal conductivity and pile thermal resistance are compared to corresponding 3D FEM model estimates.

Interpretations based on infinite source 2D finite element models do not yield reliable conductivity and resistance estimates, in the present case up to 22% discrepancy for soil thermal conductivity and 9% for pile thermal resistance. The models that do not account for the transient thermal behaviour of the pile and, in particular, the models that do not consider the pile length, consistently overestimate soil thermal conductivity and pile thermal resistance. The overestimation of pile thermal resistance is due to negative, statistical correlation between the soil and concrete thermal conductivity. The pile heat exchanger G-functions reported by [38] accurately match the thermal conductivity of the soil for the five TRTs between 60 to 150 hours. Except for the 3D FEM model, it is not possible to obtain reliable estimates of the thermal resistance of the pile with the simpler heat flow models. This is likely caused by 3D effects influencing the pile thermal resistance. Moreover, the simpler heat flow models assume a circular rather than square cross section the energy pile. To overcome this issue, potential upper and lower bounds for the pile concrete thermal resistance, for a range of thermal conductivities of concrete, are computed with the 3D model.

To summarize, TRTs are useful for inferring the thermal conductivity of the soil in the dimensioning of square cross section energy pile foundations. Tests should be carried out during the geotechnical investigations where piles are driven to assess the depth of the foundation. Interpretation of TRTs must be done with pile G-functions, either for steady (G-flov) or variable (G-flovts) heating rates depending on test conditions. It is recommended that pile thermal resistance is estimated by type curves computed with 3D FEM models.

6. Acknowledgements

7. Appendix A

Table A.1: Description of models selected to evaluate the pile heat exchanger TRT data.

	Model description	Equations	Analysed time range
Analytical approaches	**Infinite line source (ILS):** Approximates the ground heat exchanger by an infinite line source with a vanishing cross section in an infinite, isotropic and homogeneous medium [52]. A constant far-field temperature is assumed.	Late-time approximation valid for $5 < \alpha \cdot t / r^2$. $$T_b(r,t) = \frac{q}{4\pi\lambda_s}\left(\ln\left(\frac{4\alpha t}{r_b^2}\right) - \gamma\right) \qquad (11)$$ where t is time and γ is Euler's constant.	Fo > 5, steady state in the pile.
	Infinite cylinder source (ICS): Approximates the ground heat exchanger by an infinite hollow cylinder in an infinite, isotropic and homogeneous medium. A specified heating rate is imposed at a radius equal to the cylinder surface wall [21] assuming a constant far-field temperature. The simplification by [53] is used.	$$T_b(r,t) = \frac{q}{2\pi\lambda_s r_b}\sum_{j=1}^{10}\left[\frac{V_j}{j}\cdot\frac{K_0(\omega_j r)}{\omega_j K_1(\omega_j r_b)}\right]; \quad (12) \qquad \omega_j(t) = \sqrt{\frac{j\ln(2)}{\alpha t}} \quad (13)$$ $$V_j = \sum_{k=\text{Int}\left(\frac{j+1}{2}\right)}^{\min(j,5)}\frac{(-1)^{j-5}k^5(2k)!}{(5-k)!(k-1)!k!(j-k)!(2k-j)!} \qquad (14)$$ where K_0 and K_1 are modified Bessel functions of the second kind of order 0 and 1, respectively.	Fo > 5, steady state in the pile.
	Infinite solid cylinder source (ISCS): Approximates the ground heat exchanger by a solid cylinder with an infinite length in an infinite, isotropic and homogeneous medium. A specified heating rate is applied at the outer surface of the cylinder and heat can dissipate radially towards the centre of the cylinder and to the soil. The analytical formulation and corresponding simplifications are given by [25]. Here, the simplified equations are used.	The approximation is valid for $(p+1)^2 \le \text{Fo} \ll \infty$. $$G(r,t) = \frac{1}{2}\left[-\gamma - \ln\frac{r^2 + r_b^2 + |r^2 - r_b^2|}{8r_b^2\text{Fo}} + \frac{1+p^2}{4\text{Fo}}\right] \qquad (15)$$ where $p = r/r_b$.	Fo > 4, transient in the pile.
	Finite solid cylinder source (FSCS): Identical to the model proposed by [25] except that the cylinder source has a finite length. The simplified approximation presented by [25] is used in the present study.	The approximation is valid for $(p+1)^2 \le \text{Fo} \ll H^2/r_b^2$. $$G = \frac{1}{2}\left[-\gamma - \ln\frac{r^2 + r_b^2 + |r^2 - r_b^2|}{8r_b^2\text{Fo}} + 3\frac{r+r_b}{H}\frac{2}{\pi}E_0(\frac{4rr_b}{(r+r_b)^2}) - \frac{3}{\sqrt{\pi}}\sqrt{\frac{4t}{t_z}} - \frac{3}{\sqrt{\pi}}\frac{r^2+r_b^2}{\sqrt{4\text{Fo}}r_bH} + \frac{p^2+1}{4\text{Fo}}\right] \qquad (16)$$ Where $p = r/r_b$, $E_0(m)$ is the complete elliptic integral of the second kind of order 0 and t_z is H^2/α.	Fo > 4, transient in the pile.

Semi-empirical approach	**G-functions for pile heat exchangers (G-flov):** Ref. [38] proposed semi-empirical functions for the transient behaviour of energy piles. The solutions are based on 3D finite element model curve fitting. The G-functions combine G-functions for the concrete G_c, which describe the temperature response inside the pile, and pile G-functions G_g, which describe the temperature response of the ground surrounding the pile. They account for different properties of the pile and the soil and have been computed for upper and lower bound temperature responses for different aspect ratios. The upper bound is defined by a large diameter pile with pipes near the edge of the pile and where the ratio between concrete and soil thermal conductivity is equal to 2. The lower bound is defined by a large diameter pile with centred pipes and where the ratio between concrete and soil thermal conductivity is equal to 0.5. G-functions take into account heating rate variations by temporal superposition and considers the finite length of the pile.	Ground temperature response G_g for upper bound solution and for lower bound solutions, for Fo > 0.1 and Fo > 0.25, respectively: $$G_g = a[\ln(Fo)]^7 + b[\ln(Fo)]^6 + c[\ln(Fo)]^5 + d[\ln(Fo)]^4 + e[\ln(Fo)]^3 + f[\ln(Fo)]^2 + +g[\ln(Fo)] + h$$ (17) Concrete G-function Gc for Fo < 10: $$G_c = a[\ln(Fo)]^6 + b[\ln(Fo)]^5 + c[\ln(Fo)]^4 + d[\ln(Fo)]^3 + e[\ln(Fo)]^2 + f[\ln(Fo)] + g \quad (18)$$ The curve fitting parameters are given in Appendix A and B in [38]. To get the average fluid temperatures, the previous equations are combined as: $$T_f = T_0 + qR_{pipe} + qR_cG_c + \frac{q}{2\pi\lambda_s}G_g \quad (19)$$	Fo > 0.1, transient in the pile.
Numerical app.	**Equivalent pipe model (EQpipe):** Simplifies the cross section of the heat exchanger to a centred pipe with an area equivalent to that of the ground heat exchanger pipes. It was first proposed by [54]. It does not consider the finite length of the ground heat exchanger but it does consider its thermal mass. The model used in this paper is the one presented in [55]. The model takes into account heating rate variations by temporal superposition.		Fo > 0, transient in the pile.
	2D horizontal cross section finite element model (2D FEM): 2D cross section model of the square energy pile. Two models are considered: single-U and double U heat exchangers. The soil domain extends to a radius of 5 m. The initial temperature is set equal to the undisturbed ground temperature measured prior to the TRT. Dirichlet boundary conditions, equal to the undisturbed temperature, are imposed on vertical boundaries. Heating is simulated by a time varying source condition imposed on the elements comprising the heat exchanger fluid. The source is equally distributed in the heat exchanger pipes. The model does not consider the finite length of the pile.		Fo > 0, transient in the pile.

8. References

[1] EPA. Space conditioning: the next frontier. The potential of advanced residential space conditioning technologies for reducing pollution and saving money. Environmental protection agency, 1993.

[2] Rogelj, J., Den Elzen, M., Höhne, N., Fransen, T., Fekete, H., Winkler, H., Schaeffer, R., Sha, F., Riahi, K. & Meinshausen, M. Paris Agreement climate proposals need a boost to keep warming well below 2 C. Nature 2016, 534, pp. 631-639. doi:10.1038/nature18307.

[3] ASHRAE. 2009 ASHRAE Handbook. Fundamentals. 1791 Tullie Circle, N.E., Atlanta, GA 30329, American Society of Heating, Refrigerating and Air-Conditioning Engineers, Inc, 2009.

[4] Oklahoma State University. Closed-loop/ground source heat pump systems. Installation guide. UNIVERSITY, O. S. (Eds.); International Ground Source Heat Pump Association, 1988. ISBN: 0-929974-01-8.

[5] Brandl, H. Energy foundations and other thermo-active ground structures. Geotechnique 2006, 56, pp. 81-122. https://doi.org/10.1680/geot.2006.56.2.81.

[6] Park, S., Lee, D., Choi, H.J., Jung, K. & Choi, H. Relative constructability and thermal performance of cast-in-place concrete energy pile: Coil-type GHEX (ground heat exchanger). Energy 2015, 81, pp. 56-66. https://doi.org/10.1016/j.energy.2014.08.012.

[7] Loveridge, F., Olgun, C.G., Brettmann, T. and Powrie, W. The thermal behaviour of three different auger pressure grouted piles used as heat exchangers. Geotechnical and Geological Engineering 2014, 33(2), pp. 273-289. doi:10.1007/s10706-014-9757-4.

[8] Brettman, T. P. E., Amis, T. & Kapps, M. Thermal conductivity analysis of geothermal energy piles. In Proceedings of the Geotechnical Challenges in Urban Regeneration Conference, London, UK, 2010.

[9] Laloui, L., & Nuth, M. Investigations on the mechanical behaviour of a Heat Exchanger Pile. In Proceedings of the Fifth International Conference on Deep Foundations On Bored and Auger Piles, , Frankfurt, Germany, 15 May 2009. Van Impe & Van Impe (Eds.); 2009, Taylor & Francis Group, London. ISBN 978-0-415-47556-3.

[10] De Groot, M., De Santiago, C. & Pardo De Santayana, F. Heating and cooling an energy pile under working load in Valencia. In Proceedings of the 23rd European Young Geotechnical Engineers Conference. Barcelona, 2013.

[11] Alberdi-Pagola, M. & Poulsen, S. E. Thermal response testing and performance of quadratic cross section energy piles (Vejle, Denmark). In Proceedings of the XVI European Conference on Soil Mechanics and Geotechnical Engineering 2015. Edinburgh, United Kingdom, September 2015. ICE Institution of Civil Engineers. doi:10.1680/ecsmge.60678.vol5.379.

[12] Pahud, D. Geothermal energy and heat storage. Cannobio: SUPSI – DCT – LEEE. Scuola Universitaria Professionale della Svizzera Italiana, 2002.

[13] Balfour Beatty Ground Engineering. Geothermal driven piles. Available online, URL: https://www.balfourbeatty.com/media/29535/geothermal-driven-piles.pdf, 2016.

[14] Park, H., Lee, S.-R., Yoon, S. & Choi, J.C. Evaluation of thermal response and performance of PHC energy pile: Field experiments and numerical simulation. Applied Energy 2013, 103, pp. 12-24. https://doi.org/10.1016/j.apenergy.2012.10.012.

[15] Jalaluddin, A. M., Tsubaki, K., Inoue, S. & Yoshida, K. Experimental study of several types of ground heat exchanger using a steel pile foundation. Renewable Energy 2011, 36, pp. 764-771. https://doi.org/10.1016/j.renene.2010.08.011.

[16] Lennon, D. J., Watt, E. & Suckling, T. P. Energy piles in Scotland. In Proceedings of the Fifth International Conference on Deep Foundations on Bored and Auger Piles, Frankfurt, Germany, 15 May 2009. Van Impe & Van Impe (Eds.); 2009, Taylor & Francis Group, London.

[17] Mogensen, P. Fluid to Duct Wall Heat Transfer in Duct System Heat Storage. In Proceedings of the International Conference On Subsurface Heat Storage in Theory and Practice, Stockholm, Sweden, June 6-8, 1983, pp. 652-657, Swedish Council for Building Research.

[18] Gehlin, S. Thermal Response Test. Method Development and Evaluation. PhD Thesis, Luleå University of Technology, Luleå, Sweden, 2002.

[19] Spitler, J. D. & Gehlin, S. E. A. Thermal response testing for ground source heat pump systems - An historical review. Renewable and Sustainable Energy Reviews 2015, 50, pp. 1125-1137. https://doi.org/10.1016/j.rser.2015.05.061.

[20] Carslaw, H. S. & Jaeger, J. C. Conduction of Heat in Solids. Clarendon Press, Oxford Science Publications 1959, UK, ISBN 0-19-853368-3.

[21] Ingersoll, L.R., Zobel, O.J. & Ingersoll, A.C. Heat Conduction With Engineering, Geological, and Other Applications. Ed. The University of Wisconsin Press, 1954 in Madison, Wisconsin.

[22] Eskilson, P. Thermal Analysis of Heat Extraction. PhD Thesis, University of Lund, Lund, Sweden, 1987.

[23] Philippe, M., Bernier, M. & Marchio, D. Validity ranges of three analytical solutions to heat transfer in the vicinity of single boreholes. Geothermics 2009, 38, pp. 407-413. https://doi.org/10.1016/j.geothermics.2009.07.002.

[24] Li, M. & Lai, A. C. K. New temperature response functions (G functions) for pile and borehole ground heat exchangers based on composite-medium line-source theory. Energy 2012, 38, pp. 255-263. https://doi.org/10.1016/j.energy.2011.12.004.

[25] Bandos, T. V., Campos-Celador, Á., López-González, L. M. & Sala-Lizarraga, J. M. Finite cylinder-source model for energy pile heat exchangers: Effects of thermal storage and vertical temperature variations. Energy, 78, 2014, pp. 639-648. http://dx.doi.org/10.1016/j.energy.2014.10.053.

[26] Li, M. & Lai, A. C. Review of analytical models for heat transfer by vertical ground heat exchangers (GHEs): a perspective of time and space scales. Applied Energy 2015, 151, pp. 178-191. https://doi.org/10.1016/j.apenergy.2015.04.070.

[27] Javed, S., Fahlén, P. & Claesson, J. Vertical ground heat exchangers: A review of heat flow models. In Proceedings of Effstock 2009, 14-17 June 2009, Stockholm, Sweden.

[28] Witte, H. J. L. Error analysis of thermal response tests. Applied Energy 2013, 109, pp. 302-311. https://doi.org/10.1016/j.apenergy.2012.11.060

[29] Signorelli, S., Bassetti, S., Pahud, D. & Kohl, T. Numerical evaluation of thermal response tests. Geothermics 2007, 36, pp. 141-166. https://doi.org/10.1016/j.geothermics.2006.10.006.

[30] Loveridge, F.A., Brettmann, T., Olgun, C.G. & Powrie, W. Assessing the applicability of thermal response testing to energy piles. At Global Perspectives on the Sustainable Execution of Foundations Works, Sweden, 21-23 May 2014.

[31] Loveridge, F. The thermal performance of foundation piles used as heat exchangers in ground energy systems. PhD Thesis, University of Southampton, Southampton, UK, 2012.

[32] GSHP Association. Thermal Pile: Design, Installation & Materials Standards. National Energy Centre, Davy Avenue, Knowlhill, Milton Keynes. Ground Source Heat Pump Association, 2012.

[33] Loveridge, F., Powrie, W. & Nicholson, D. Comparison of two different models for pile thermal response test interpretation. Acta Geotechnica 2014, 9, pp. 367-384. https://doi.org/10.1007/s11440-014-0306-3.

[34] Hu, P., Zha, J., Lei, F., Zhu, N. & Wu, T. A composite cylindrical model and its application in analysis of thermal response and performance for energy pile. Energy and Buildings 2014, 84, pp. 324-332. https://doi.org/10.1016/j.enbuild.2014.07.046.

[35] Yu, K., Singh, R., Bouazza, A. & Bui, H. Determining soil thermal conductivity through numerical simulation of a heating test on a heat exchanger pile. Geotechnical and Geological Engineering 2015, 33, pp. 239-252. https://doi.org/10.1007/s10706-015-9870-z.

[36] Badenes, B., De Santiago, C., Nope, F., Magraner, T., Urchueguía, J., De Groot, M., Pardo DE Santayana, F., Arcos, J. L. & Martín, F. Thermal characterization of a geothermal precast pile in Valencia (Spain). In Proceedings of the European Geothermal Congress 2016, Strasbourg, France, 19-24 September 2016.

[37] Zarrella, A., Emmi, G., Zecchin, R. & De Carli, M. An appropriate use of the thermal response test for the design of energy foundation piles with U-tube circuits. Energy and Buildings 2017, 134, pp. 259-270. https://doi.org/10.1016/j.enbuild.2016.10.053.

[38] Loveridge, F. & Powrie, W. Temperature response functions (G-functions) for single pile heat exchangers. Energy 2013, 57, pp. 554-564. https://doi.org/10.1016/j.energy.2013.04.060.

[39] Alberdi-Pagola, M., Jensen, R. L. & Poulsen, S. E. A performance case study of energy pile foundation at Rosborg Gymnasium (Denmark). In Proceedings of the 12th REHVA World Congress Clima 2016, 22-25 May 2016 Aalborg, Denmark. Department of Civil Engineering, Aalborg University, pp. 10.

[40] Centrum Paele A/S. Energipæle, 2002 [Online]. Available: http://www.centrumpaele.dk/paele/energipaele.html [Accessed 03-08-2017].

[41] Bourne-Webb, P., Bernard, J.-B., Friedemann, W., Von Der Hude, N., Pralle, N., Uotinen, V. M. & Widerin, B. Delivery of Energy Geostructures. In Energy Geostructures, Laloui, L. and Di Donna, A. (Eds.); John Wiley & Sons, Inc., 2013.

[42] Alberdi-Pagola, M., Poulsen, S. E., Jensen, R. L. & Madsen, S. Thermal response testing of precast pile heat exchangers: fieldwork report. In: Aalborg University, Department of Civil Engineering (Eds.); Aalborg, Denmark, 2016.

[43] Alberdi-Pagola, M. Thermal Response Test data of five quadratic cross section precast pile heat exchangers. Data in Brief 2017, submitted.

[44] Hot Disk AB. Hot Disk Thermal Constants Analyser TPS 1500 unit. Instruction Manual. 2014.

[45] COMSOL Multiphysics. COMSOL Multiphysics version 5.1: user's guide. In: COMSOL (Eds.). Burlington, 2015.

[46] COMSOL Multiphysics. Pipe Flow Module - User's guide. In: COMSOL (Eds.). 2012.

[47] Churchill, S. W. Friction factor equations spans all fluid-flow regimes. Chemical Engineering Journal, 1977, 84, pp. 94-95.

[48] Abdelaziz, S. L. A. M. Deep energy foundations: geotechnical challenges and design considerations. PhD Thesis, Virginia Polytechnic Institute and State University, 2013.

[49] Loveridge, F. & Cecinato, F. Thermal performance of thermoactive continuous flight auger piles. Environmental Geotechnics 2016, 3(4), pp. 265-279.

[50] Al-Khoury, R. Computational modeling of shallow geothermal systems. Leiden, The Netherlands: CRC Press; 2011.

[51] Spitler, J.D. & M. Bernier. Vertical borehole ground heat exchanger design methods. In Advances in Ground-Source Heat Pump Systems; Rees, S. J. (Eds.); Woodhead Publishing, 2016.

[52] Kelvin, T. W. Mathematical and physical papers. Cambridge University Press, London, 1882.

[53] Baudoin, A. Stockage intersaisonnier de chaleur dans le sol par batterie d'échangeurs baïonnette verticaux modèle de prédimensionnement. PhD Thesis, Université de Reims, France, 1988.

[54] Shonder, J. A. & Beck, J. V. Field test of a new method for determining soil formation thermal conductivity and borehole resistance. ASHRAE Transactions 2000, 106, pp. 843-850.

[55] Poulsen, S. E. & Alberdi-Pagola, M. Interpretation of ongoing thermal response tests of vertical (BHE) borehole heat exchangers with predictive uncertainty based stopping criterion. Energy 2015, 88, 157-167. https://doi.org/10.1016/j.energy.2015.03.133.

[56] Doherty, J. PEST Model-Independent Parameter Estimation. User Manual, Watermark Numerical computing, 2010, http://www.pesthomepage.org/Downloads.php.

[57] Dansk Geoteknik A/S, Geoteknisk rapport. Grundundersøgelser for Amtsgymnasium i Vejle, Vestre Engvej, Vejle. 1973.

[58] Austin, W. A. Development of an in-situ system and analysis procedure for measuring ground thermal properties. ASHRAE Transactions 2000, 106 (1), pp. 365-379.

[59] Witte, H. J. L., Gelder, G. J. V. & Spitler, J. D. In Situ Measurement of Ground Thermal Conductivity: A Dutch Perspective. ASHRAE Transactions 2002, 108, pp. 263-272.

[60] Low, J. E., Loveridge, F. A., Powrie, W. & Nicholson, D. A comparison of laboratory and in situ methods to determine soil thermal conductivity for energy foundations and other ground heat exchanger applications. Acta Geotechnica 2014, 10, pp. 209-218. https://doi.org/10.1007/s11440-014-0333-0.